Research Article **Open Access**

Yevgen Gorash* and Donald MacKenzie

On cyclic yield strength in definition of limits for characterisation of fatigue and creep behaviour

DOI 10.1515/eng-2017-0019
Received April 8, 2015; accepted September 4, 2015

Abstract: This study proposes cyclic yield strength as a potential characteristic of safe design for structures operating under fatigue and creep conditions. Cyclic yield strength is defined on a cyclic stress-strain curve, while monotonic yield strength is defined on a monotonic curve. Both values of strengths are identified using a two-step procedure of the experimental stress-strain curves fitting with application of Ramberg-Osgood and Chaboche material models. A typical S-N curve in stress-life approach for fatigue analysis has a distinctive minimum stress lower bound, the fatigue endurance limit. Comparison of cyclic strength and fatigue limit reveals that they are approximately equal. Thus, safe fatigue design is guaranteed in the purely elastic domain defined by the cyclic yielding. A typical long-term strength curve in time-to-failure approach for creep analysis has two inflections corresponding to the cyclic and monotonic strengths. These inflections separate three domains on the long-term strength curve, which are characterised by different creep fracture modes and creep deformation mechanisms. Therefore, safe creep design is guaranteed in the linear creep domain with brittle failure mode defined by the cyclic yielding. These assumptions are confirmed using three structural steels for normal and high-temperature applications. The advantage of using cyclic yield strength for characterisation of fatigue and creep strength is a relatively quick experimental identification. The total duration of cyclic tests for a cyclic stress-strain curve identification is much less than the typical durations of fatigue and creep rupture tests at the stress levels around the cyclic yield strength.

Keywords: creep, cyclic plasticity, fatigue life, fatigue limit, failure, plasticity, steel, yield strength.

***Corresponding Author: Yevgen Gorash:** Department of Mechanical and Aerospace Engineering, University of Strathclyde, Glasgow G1 1XJ, Scotland, United Kingdom,
E-mail: yevgen.gorash@strath.ac.uk, Phone: +44 141 444 7969
Donald MacKenzie: Department of Mechanical and Aerospace Engineering, University of Strathclyde, Glasgow G1 1XJ, Scotland, United Kingdom, E-mail: d.mackenzie@strath.ac.uk

1 Introduction

Characterisation of long-term strength of structural materials is an important engineering task for prevention of potential catastrophic failures of critical equipment. However, studies of this type are usually very long-lasting, technically challenging and involve expensive experimental work. Thus, the main scope of this study is the formulation of a simple way to predict characteristics of the long-term material behaviour under creep and fatigue conditions using basic material properties. Based upon the extensive availability of experimental material data, a significant progress toward this challenge has been achieved so far and may be observed in the literature as indicated below.

One should start with the fundamental work of Bäumel and Seeger [1], who discussed a few methods for estimating fatigue behaviour of metals using strain-life approach on the basis of monotonic test results. They included the Method of Universal Slopes (MUS) proposed by Manson [2] and modification of MUS developed by Muralidharan & Manson [3], which are applicable to all metals. However, this approach contained a critical limitation regardless of a good accuracy, which is the requirement of reduction in area ψ availability.

The flaw of MUS formulations induced Bäumel and Seeger [1] to develop the Uniform Material Law (UML) using as its basis the extensive collection of fatigue data [4] with over 1500 experimental results. Unalloyed and low-alloy steels were analysed separately from aluminium and titanium alloys resulting into two sets of equations both being based on only elasticity modulus E and ultimate tensile strength (UTS) σ_u, which can be easily correlated with Vickers hardness HV. Later, the applicability of UML concept was extended to high-strength steels by Korkmaz [5].

Comparative study by Kim *et al.* [6] evaluated seven basic methods for estimating uniaxial fatigue properties (including fatigue limit σ_{lim}^{f}) from tensile properties or hardness. This study was based upon the fatigue test data for eight ductile steels under axial and torsional loading. Three of the evaluated methods were able to predict over 93% of the test cases within a factor of 3 compared to the

observed lives. The formulas for σ^{f}_{lim} prediction included mechanical properties such as E, σ_u and true fracture ductility ε_f. Among the variety of empirical formulations for σ^{f}_{lim} prediction with different combinations of aforementioned mechanical properties, the simplest are based on σ_u: $\sigma^{f}_{lim} = 1.9018\,\sigma_u$ (MUS); $\sigma^{f}_{lim} = 1.5\,\sigma_u$ (UML); and $\sigma^{f}_{lim} = \sigma_u + 345$ MPa (Mitchell's method), which showed an accuracy of $R^2 = 0.88$. Another simple method in this comparison, proposed by Roessle & Fatemi [7], used a Brinnell hardness HB for prediction as $\sigma^{f}_{lim} = 4.25\,HB + 225$ MPa. This approach showed a reasonable accuracy of $R^2 = 0.86$ for the experimental data fit.

Casagrande *et al.* [8] investigated a relationship between σ^{f}_{lim} and Vickers hardness HV in steels and developed a method to predict σ^{f}_{lim}. A good correlation was observed between HV and σ^{f}_{lim} for four kinds of steels in different metallurgical states. However, the proposed empirical method is not straightforward and involves a number of parameters and equations to achieve a reasonable of accuracy of σ^{f}_{lim} predictions. Recently, Bandara *et al.* [9] proposed a formula for predicting σ^{f}_{lim} of steels in the Giga-Cycle Fatigue (GCF) regime. It uses a combination of σ_u and HV as material parameters and was verified using the experimental results for 45 steels.

An alternative approach was suggested by Li *et al.* [10], who estimated theoretically the cyclic yield strength σ^{c}_{y} and σ^{f}_{lim} using the test data for 27 alloy steels. One formula expresses σ^{c}_{y} by two conventional mechanical performance parameters – σ_u and the reduction in area ψ. The other formula expresses the fatigue endurance limit through the cyclic yield strength with a reasonable accuracy of $R^2 = 0.883$ as $\sigma^{f}_{lim} = 1.13\,(\sigma^{c}_{y})^{0.9}$. Despite the relative simplicity, the proposed relation can't be considered as mathematically elegant, most probably because of the conventional assumption of 0.2% plastic strain offset for yield strength. Nevertheless, this formula by Li *et al.* [10] demonstrated the tendency that σ^{f}_{lim} is not very different from σ^{c}_{y}.

A computational approach was developed by Tomasella *et al.* [11], who applied the Artificial Neural Networks to estimation of the cyclic material properties used in strain-life fatigue approach from a set of monotonic material properties. This approach was implemented into the software called Artificial Neural Strain Life Curves (ANSLC), and has been tested on a large database of steels [1, 4]. In comparison with the largely used UML [1], the results of the estimation with ANSLC program, even without including the support of real experimental tests in the regression, showed a considerably higher accuracy in the life-time estimation.

Recently, Pang *et al.* [12] did a comprehensive review of the relations between σ^{f}_{lim} and other mechanical properties of metallic materials. They include the qualitative / quantitative relations between σ^{f}_{lim} and hardness (HV or HB), strength (σ_u and σ_y) and toughness. Analysis of the numerous fatigue data resulted in the General Fatigue Formula (GFF): $\sigma^{f}_{lim} = \sigma_u\ (C - P \cdot \sigma_u)$, where C and P are fitting parameters. GFF was found applicable to σ^{f}_{lim} prediction with increasing σ_u in a wide range for many materials such as conventional metals and newly developed alloys. Pang *et al.* [12] suggested that GFF can provide a new clue to predict σ^{f}_{lim} and select the appropriate materials within engineering design by adjusting parameters P and C adequately.

The concept of the fatigue limit σ^{f}_{lim} has been comprehensively studied on microstructural scale by Bathias [13]. This experimental and theoretical study was based upon a thorough and authoritative examination of the coupling between plasticity, crack initiation and heat dissipation for lifetimes that exceed the billion cycle. Moreover, the validity of GCF concept was proved, what questions the idea of infinite fatigue life, at least for practical applications.

Less progress has been achieved in the methods for creep rupture strength evaluation, but recently an important observation was discovered by Kimura [14]. The creep strength of ferritic and austenitic steels has been investigated in [14] through the correlation between creep rupture curve, presenting stress vs. creep rupture life, and 50% of 0.2% offset yield stress (half yield) at a wide range of temperatures. The inflection of the creep rupture curve at half yield was recognised for ferritic creep resistant steels with martensitic or bainitic microstructure, e.g. T91, T92 and T122. This was explained in terms of different mechanisms of microstructural evolution during creep at high- and low-stress regimes. The purpose of this study was to point out a significant risk of overestimation of long-term creep rupture strength by extrapolating the data for martensitic and bainitic steels (e.g. ASTM T91/P91) in high-stress regime to low-stress regime, which are separated by half yield.

A similar problem with particular application to ASTM P91 steel was investigated and discussed earlier by Gorash *et al.* [15–17] for the purpose of a creep constitutive model development. In these works, apart from inflection of the creep rupture curve, the simultaneous inflection of the minimum creep rate curve, presenting minimum creep rate vs. stress, was recognised. Alternation of the minimum creep rate slope was explained in terms of different creep deformation mechanism (linear creep for low stress and power-law for high stress), while alternation of the creep rupture life slope was explained in terms of different damage accumulation modes (brittle fracture for low

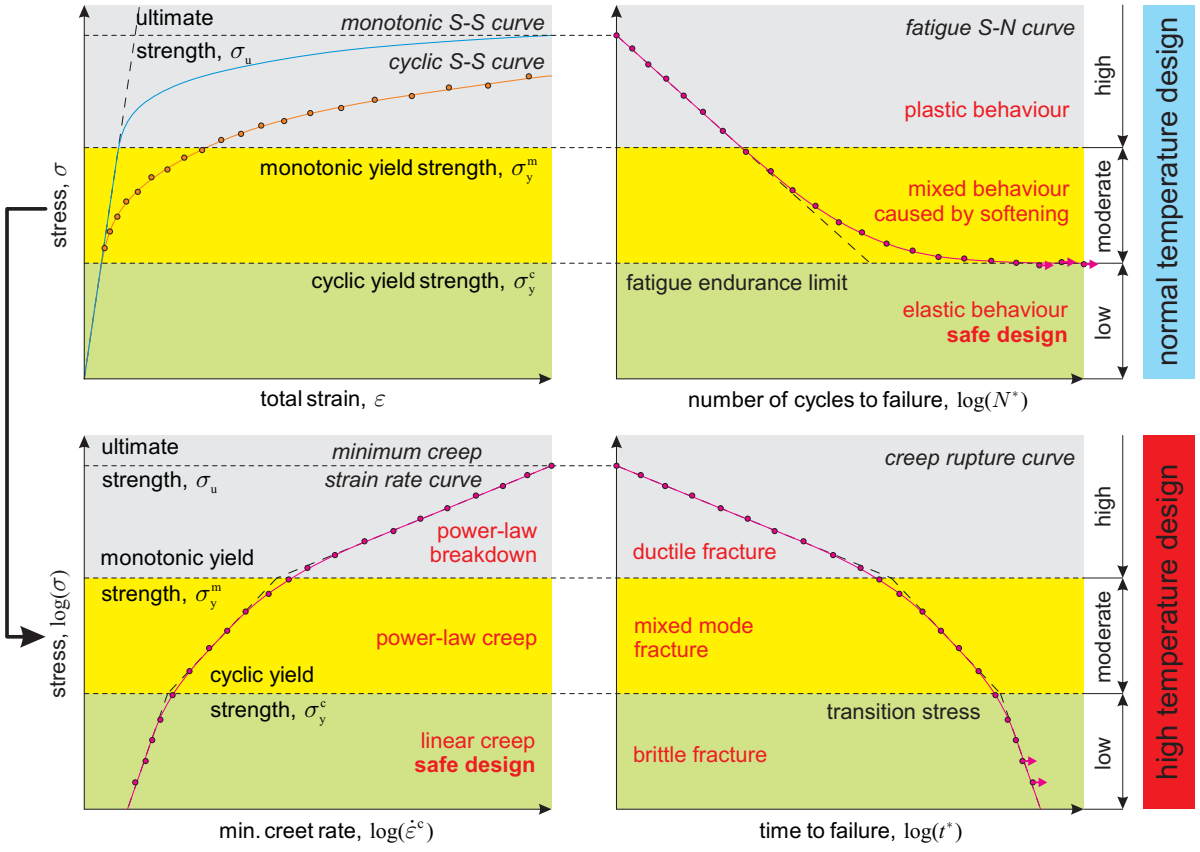

Figure 1: Concept of the safe structural design for fatigue and creep using cyclic yield strength.

stress and ductile for high stress). The inflection of both curves was characterised by the same value $\sigma_\star^{cr}$ called transition stress, which had the meaning of material parameter in the developed "double power law" creep model. However, $\sigma_\star^{cr}$ was identified in [15–17] using the minimum creep rate data, and no relation of $\sigma_\star^{cr}$ to basic mechanical properties of ASTM P91 steel was recognised.

The principal aim of the present study is to investigate a link in characterisation of long-term strength of structural steel by finding a similar quantative feature in available experimental data. This work establishes relationships between characteristics of creep and fatigue behaviour on one hand and yield strength as a basic material property and characteristic of plasticity on other hand.

2 Concept of the safe structural design

2.1 Definition of the yield strength

Dowling [18] discusses several methods to characterise the yield strength σ_y. The first is the *proportional limit* σ_y^p, which is the stress where the first departure from linearity occurs. The second is the *elastic limit* σ_y^{el}, which is the highest stress that does not cause plastic deformation. The third is the *offset yield strength* $\sigma_y^{0.2\%}$, which is the stress in the point on stress-strain curve typically defined by the plastic strain offset of 0.2% from elastic line. This value is generally the most practical means of defining the yielding event for engineering metals. Therefore, $\sigma_y^{0.2\%}$ is usually meant to define the yield strength σ_y in the literature. However, here the *elastic limit* σ_y^{el}, defined in the scope of unified Chaboche model [19, 20], is used as the yield strength σ_y.

This study proposes the cyclic yield strength σ_y^c as a key characteristic for the definition of safe design for engineering structures operating under fatigue and creep con-

ditions, as illustrated in Fig. 1. It is conventionally defined in context of a cyclic stress-strain curve (SSC), which is obtained from results of cyclic tests for a number of different strain ranges. Each cyclic test produces a stabilised stress response, which is affected either by hardening or by softening depending on the type of steel. In case of steels with a cyclic softening effect, σ_y^c separates the low stress range of purely elastic behaviour from the moderate stress range of mixed elasto-plastic behaviour. Monotonic yield strength σ_y^m, which is conventionally defined in context of a monotonic SSC, separates the moderate stress range of mixed elasto-plastic behaviour from the high stress range of purely plastic behaviour. Both values of σ_y^m and σ_y^c are identified using a 2-steps fitting procedure of the experimental stress-strain curves. The first step applies the Ramberg-Osgood material model, which produces basic smoothing and extrapolation, to the both monotonic and cyclic SSCs separately. The second step of fitting involves a typical rate-independent form of the Chaboche material model with 3 kinematic backstresses. Fitting the Chaboche model with two separate sets of material constants sequentially to the both SSCs provides the values of σ_y^m and σ_y^c with minimum offset from the elastic line as elastic limits.

2.2 Stress-strain curves fitting procedure

As experimental SSCs usually demonstrate some level of scatter, the first step in data fitting for the material parameters identification is the basic curve smoothing. The conventional Ramberg-Osgood (R-O) equation [24] is optimal for such curve smoothing since it was formulated to describe the non-linear relationship between stress and strain in materials near their yield point. It is particularly useful for metals that harden or soften with plastic deformation showing a smooth elastic-plastic transition. The equations for monotonic and cyclic SSCs are:

$$\varepsilon^{tot} = \frac{\sigma}{E} + \left(\frac{\sigma}{B}\right)^{1/\beta} \quad \text{and} \quad \frac{\Delta\varepsilon^{tot}}{2} = \frac{\Delta\sigma}{2E} + \left(\frac{\Delta\sigma}{2B}\right)^{1/\beta}, \tag{1}$$

where $\Delta\varepsilon_{tot}$ is the total strain range and $\Delta\sigma$ is the total stress range (MPa) for each cyclic test respectively; B and β are the R-O material parameters; and Young's modulus E in MPa. Using the value of E, the total strain ε^{tot} in the experimental curves is decomposed into elastic and plastic strain. Then the plastic component ε^p of strain is fitted using the the least squares method by the following power-law relations, which are derived from the Eq. (1):

$$\sigma = B\left(\varepsilon^p\right)^{\beta} \quad \text{and} \quad \frac{\Delta\sigma}{2} = B\left(\frac{\Delta\varepsilon^p}{2}\right)^{\beta}. \tag{2}$$

The resultant R-O fits for monotonic and cyclic curves are then used to identify the parameters for the Chaboche material model. The range of applicability for the R-O fit is usually quite narrow not exceeding 1% of ε^{tot} depending on the grade of curvature grade for a SSC.

The basic variant of the rate-independent Chaboche model [19, 20] is presented as a combination of nonlinear kinematic hardening and nonlinear isotropic hardening models. The model allows the superposition of several independent backstress tensors and can be combined with any of the available isotropic hardening models. Since in this study monotonic and cyclic SSCs are fitted separately only for the identification of σ_y, only the kinematic hardening component is considered:

$$X = \sum_{i=1}^{N} X_i, \quad \text{with} \quad \dot{X}_i = C_i\,\dot{\varepsilon}^p - \gamma_i X_i\,\dot{p}, \tag{3}$$

where $\dot{\varepsilon}^p$ is the plastic strain rate, and $\dot{p}$ is its magnitude. The total backstress X in Eq. (3) is given by the superposition of a number N of kinematic backstresses X_i with a corresponding evolution equation initially proposed by by Armstrong & Frederick [25] for $\dot{X}_i$, where C_i and γ_i are kinematic material constants. Chaboche *et al.* [19] recommended $N = 3$ in order to provide a good fit of experimental SSCs, which include large strain areas. Therefore, three backstresses are considered in this study providing an excellent match of the R-O fit (1) for a whole range of strains.

The kinematic hardening constants (C_i, γ_i) and σ_y, which define the size of the yield surface, are identified as recommended in [20]. The cyclic SSC is fitted by the following relation:

$$\frac{\Delta\sigma}{2} = \sigma_y^c + \sum_{i=1}^{N} \frac{C_i}{\gamma_i} \tanh\left(\gamma_i \frac{\Delta\varepsilon^p}{2}\right), \tag{4}$$

which is obtained in [20] by integrating Eq. (3) and considering $\varepsilon^p \approx$ const at the peak stresses for strain-controlled cyclic loading. Relation (4) is valid for the cyclic curve after stabilisation of the hardening or softening effects. Constants (C_i, γ_i and cyclic σ_y^c) are identified by automatic fitting Eq. (4) to the R-O extrapolation (2) with "cyclic" values of constants B and β. The identification procedure is implemented in Microsoft Excel using an add-in Solver [26]. The Solver searches for an optimal (minimum in this case) value for a formula in one cell – called the objective cell – subject to constraints, or limits, on the values of other formula cells on a worksheet. The Solver works with a group

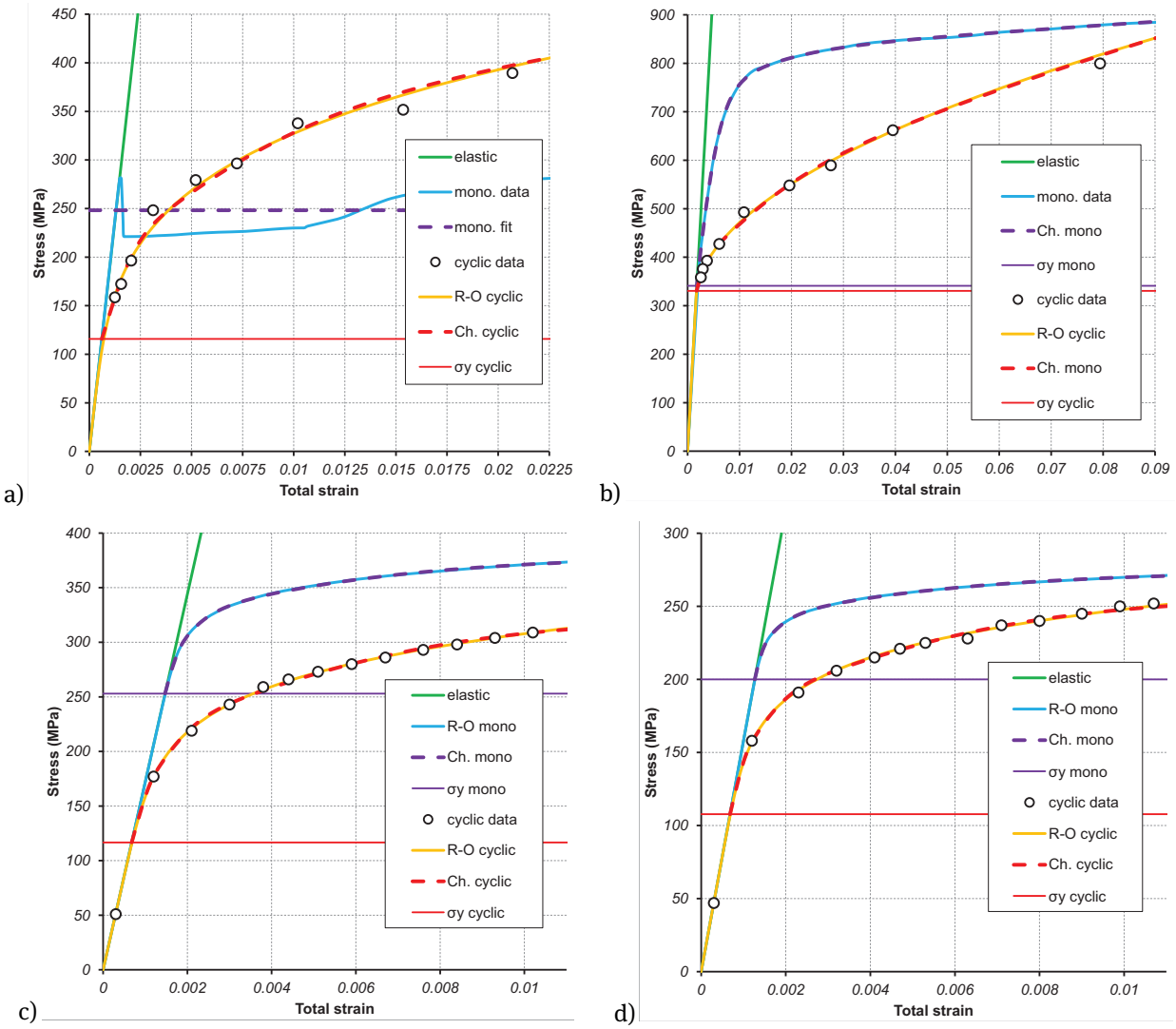

Figure 2: Fitting of monotonic and cyclic SSCs for: a) ASTM A36 steel from [21] at RT; b) AISI 4340 steel from [22] at RT c) ASTM P91 steel from [23] at 550°C and d) at 600°C.

of cells, called decision variables or simply variable cells, that participate in computing the formulas in the objective and constraint cells. In this case, the Solver adjusts the values in the decision variable cells containing material constants (C_i, γ_i and σ_y^c) in order to minimise the value in the objective cell. This cell contains an average value of the absolute difference between columns containing $\frac{\Delta\sigma}{2}$ calculated by Eq. (2) and Eq. (4) correspondingly in a particular range of $\Delta\varepsilon^p$. Applying this approach, an excellent match of Eqs (2) and (4) is achieved.

The monotonic SSC is fitted by the different relation in the following form [20]:

$$\sigma = \sigma_y^m + \sum_{i=1}^{N} \frac{C_i}{\gamma_i} \left[1 - \exp(-\gamma_i \varepsilon^p)\right], \tag{5}$$

which contains the monotonic σ_y^m and different values of kinematic hardening constants (C_i, γ_i). These constants are identified by fitting Eq. (5) to the R-O extrapolation (2) with "monotonic" values of the R-O parameters B and β. The identification procedure is implemented in Microsoft Excel using an add-in Solver in the same way as for cyclic SSC. An advanced step-by-step guideline for the estimation of the Chaboche viscoplasticity model parameters with their further optimisation was developed by Hyde *et al.* [27].

2.3 Application to three structural steels

The above described fitting procedure is applied to SSCs of three structural steels for the purpose of σ_y^m and σ_y^c

Table 1: Fitting parameters of the Ramberg-Osgood model (1) and (6) for different steels and temperatures

Type of plastic material response	Elasto-plastic constants			
	E (MPa)	B (MPa)	β	σ_y (MPa)
ASTM A36 RT cycl.	189606	1015.61	0.2362	–
AISI 4340 RT cycl.*	193053	1897.94	0.5175	320
ASTM P91 RT mono.	215000	710	0.047	–
ASTM P91 RT cycl.		1180	0.155	–
ASTM P91 500°C m.	180000	594	0.066	–
ASTM P91 500°C c.		763	0.15	–
ASTM P91 550°C m.	172000	482	0.054	–
ASTM P91 550°C c.		613	0.144	–
ASTM P91 600°C m.	158000	330	0.042	–
ASTM P91 600°C c.		446	0.123	–
ASTM P91 650°C m.	140000	269	0.071	–
ASTM P91 650°C c.		343	0.125	–

* Extended version of the R-O model (6) is used for data fitting.

identification. The first is ASTM A36 steel, with mechanical properties available in [28] and [21], which is a standard low carbon steel, without advanced alloying and is a principal carbon steel employed for bridges, buildings, and many other structural uses. The monotonic SSC for this steel at room temperature (RT) shown in Fig. 2a exhibits perfectly plastic behaviour when reaching the stress of 36 ksi = 248.211 MPa in average, which is considered as σ_y^m. The perfectly plastic yielding lasts for approximately of $\varepsilon^p = 1$ (%) of strain plateau, which is followed by the strain hardening area, then gradually approaching failure at $\varepsilon^{tot} = 30$ (%). The cyclic SSC for this steel shown in Fig. 2a from [21] is fitted by the 2-step procedure, and the obtained material parameters for the R-O (1) and Chaboche (3)-(5) models are listed in Tables 1 and 2 correspondingly.

The second material is AISI 4340 steel [22], a high-strength alloy steel, which has good machinability features and used for a wide range of applications including aircraft landing gears, shafts or axels for power transmission, gears, high pressure pump housings, etc. Both monotonic and cyclic SSCs shown in Fig. 2b and mechanical properties are taken from [22]. Since it is available explicitly, the monotonic SSC is fitted by the Chaboche model (5) directly, and the material parameters are listed in Table 2. The cyclic SSC for this steel shown in Fig. 2b from [22] is available at ten times wider strain range than for the ASTM A36 steel. Therefore, the R-O model (1) is not able to provide an accurate fit of the cyclic SSC. In this case, the following modification of the R-O equation (1) proposed by Lemaitre & Chaboche [29] is used for fitting analysis:

$$\varepsilon^{tot} = \frac{\sigma}{E} + \left(\frac{\sigma - \sigma_y}{B}\right)^{1/\beta} \quad \text{and} \quad \frac{\Delta\varepsilon^{tot}}{2} = \frac{\Delta\sigma}{2E} + \left(\frac{\Delta\sigma - \sigma_y}{2B}\right)^{1/\beta}, \tag{6}$$

Compared to Eq. (1), this notation contains an additional parameter of the yield strength σ_y in the meaning of σ_y^{el}, and can be applied for an accurate fitting of much wider strain range than Eq. (1). Thus, the cyclic SSC is fitted by the 2-step procedure. The obtained material parameters for the modified R-O (6) and Chaboche (3)-(5) models are listed in Tables 1 and 2 correspondingly.

The third material is ASTM P91 (modified 9Cr-1Mo) steel [23, 30], an advanced ferritic steel with martensitic microstructure, which has already been widely used over the last 2 decades as tubes/pipes for heat exchangers, plates for pressure vessels, and other forged, rolled and cast components for high temperature services. Both monotonic and cyclic SSCs shown in Figs 2c and 2d and mechanical properties at room temperature (RT), 500°C, 550°C, 600°C and 650°C are taken from [23]. Firstly, the monotonic SSCs are presented in [23] by the material parameters for the R-O model (1) listed in Table 1. The cyclic SSCs are presented in [23] by raw data, which is fitted by the R-O model (1) with material parameters listed in Table 1. Secondly, both monotonic and cyclic R-O extrapolations are fitted by the Chaboche model (3)-(5) with material parameters listed in Table 2.

Table 2: Fitting parameters of the Chaboche model (3)-(5) for different steels and temperatures

Type of plastic material response	Three kinematic hardening backstresses						Yield σ
	C_1 (MPa)	γ_1	C_2 (MPa)	γ_2	C_3 (MPa)	γ_3	σ_y (MPa)
ASTM A36 RT cycl.	87345.7	984.7	14013.4	111.78	3918.32	13.477	115.792
AISI 4340 RT mono.	205524.6	535.8	8966.94	92.268	782.893	1.0739	341.153
AISI 4340 RT cycl.	35912.1	650.7	6972.29	53.297	4221.72	5.7356	330.727
ASTM P91 RT mono.	1120466	23911	125301.9	2539.9	17295.23	227.86	406.098
ASTM P91 RT cycl.	1030320	11608	136282.4	1254.6	29535.03	148.08	197.493
ASTM P91 500°C m.	1059420	23359	122317.7	2469.7	17631.89	219.49	270.687
ASTM P91 500°C c.	659430	11229	87028.5	1248.7	19146.80	149.22	134.541
ASTM P91 550°C m.	1059420	23359	122317.7	2469.7	17631.89	219.49	270.687
ASTM P91 550°C c.	659430	11229	87028.5	1248.7	19146.80	149.22	134.541
ASTM P91 600°C m.	511703	24975	56536.0	2630.3	7588.97	232.90	199.970
ASTM P91 600°C c.	444752	12216	11344.6	160.13	56238.9	1347.6	107.731
ASTM P91 650°C m.	498277	23543	56252.6	2433.8	8263.19	217.10	115.346
ASTM P91 650°C c.	353928	12801	44816.6	1396.6	8916.41	162.14	80.6307

Table 3: Material parameters of the S-N curves for ASTM A36, AISI 4340 and ASTM P91 steels.

Steel	σ_u	σ_y^c/σ_y^m	f_1	f_2	f_3
ASTM A36 RT	413.7	115.8	0.23405	4778.8	1.0
AISI 4340 RT	827.4	330.7	33.187	2955.7	0.3795
ASTM P91 RT	658.0	406.1	29.037	10258	0.5154
ASTM P91 400°C	534.0	[350]*	28.827	10303	0.4738
ASTM P91 550°C	380.0	[0.0]**	0.0375	7806.7	1.1472

* σ_y^m is not available, hence σ_{lim}^f from [35] is used.
** no σ_{lim}^f is observed at high temperatures because of creep.

3 Relation in mechanical characteristics

The next step is a search for possible correlations between the experimentally obtained yield strength values (σ_y^m and σ_y^c) for ASTM A36, AISI 4340 and ASTM P91 steels and their fatigue and creep behaviour characteristics. This identifies a clear similarity for characteristic transition stresses in S-N fatigue, minimum creep strain rate and creep rupture curves, as explained below.

3.1 Fatigue behaviour at normal temperature

Engineering structures operating under cyclic loading conditions at normal temperature are usually designed against the fatigue failure using the conventional stress-life approach. This approach involves experimental fatigue S-N curves with a number of cycles to failure $N_\star$ vs. stress. A typical S-N curve is a straight line in double logarithmic coordinates, which conventionally described by the Basquin model [36]. Referring to [18, 27], a distinctive minimum stress lower bound, which is called a fatigue endurance limit σ_{lim}^f, is observed on S-N curves for a number of structural steels with polished surface of a specimen in benign (non-corrosive and RT) environment. Referring to [13], fatigue limit, endurance limit and fatigue strength are all expressions used to describe a property of materials under cyclic loading: the amplitude (or range) of cyclic stress that can be applied to the material without causing fatigue failure. In these cases, a number of cycles (usually 10^7) are chosen to represent the fatigue life of the material.

Comparison of σ_y^c defined as a material constant and experimentally observed σ_{lim}^f reveals that they are close. This assumption is confirmed by the high-cycle fatigue (HCF) experimental data for ASTM A36 [31] and AISI 4340 [32–34] steels shown in Fig. 3. Comparison of σ_{lim}^f with σ_y^c summarised in Table 4 for ASTM A36 steel gives 27.6% accuracy and 5.5% accuracy for AISI 4340 steel. These observations indicate that the safe fatigue design is guaranteed in the purely elastic domain defined by σ_y^c.

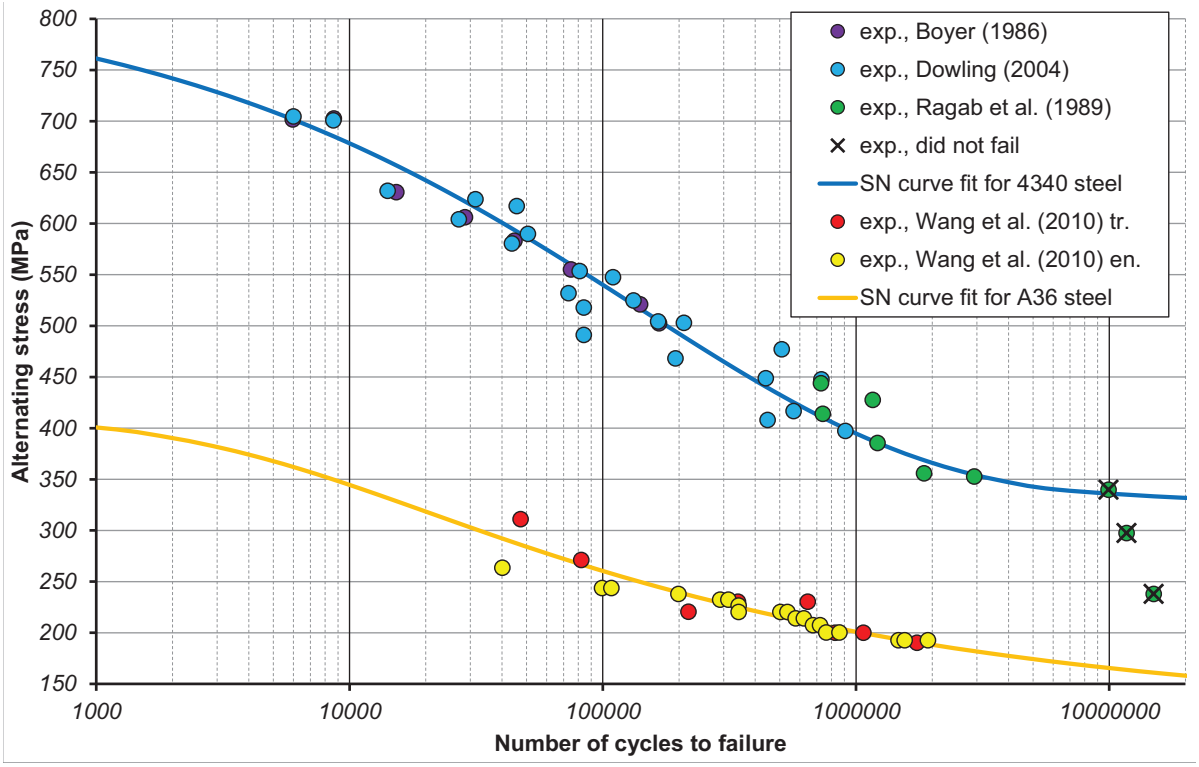

Figure 3: S-N curve fits of ASTM A36 steel based on HCF data by [31] and AISI 4340 steel based on HCF data by [32], [33] and [34]

In general, each S-N curve exhibits two limits: one, when stress tends towards the static fracture σ_u (fracture in a quarter of the cycle), and the other, when stress tends towards the fatigue limit σ_{lim}. The most known concepts able to describe a reverse sigmoidal shape of a generic S-N curve are presented by two models. The conventional one is the Bastenaire model [37, 38]:

$$N_\star = \frac{A}{\sigma_a - \sigma_{lim}^f} \exp\left[-\left(\frac{\sigma_a - \sigma_{lim}^f}{B}\right)^C\right], \tag{7}$$

where σ_a is an alternating stress. Three material parameters A, B, C and fatigue limit σ_{lim} are derived from fitting the experimental raw data.

A more advanced formulation was developed by Lemaitre & Chaboche [29] using the damage mechanics approach:

$$N_\star = \frac{\sigma_u - \sigma_{max}}{a\left[(\sigma_{max} - \bar{\sigma}) - \sigma_{lim}^f(1 - b\,\bar{\sigma})\right]} \cdot \left[\frac{\sigma_{max} - \bar{\sigma}}{c\,(1 - b\,\bar{\sigma})}\right]^{-\alpha}, \tag{8}$$

where $\bar{\sigma}$ is the mean stress of the cycle; σ_{max} is the maximum stress in the cycle; and the other variables are material parameters defined in the material property set: a – non-linear damage sensitivity, b – mean stress correction factor, c – the Chaboche equation coefficient, and α – the Chaboche equation exponent. Because the Chaboche concept incorporates its own mean stress $\bar{\sigma}$ correction [29] resembling the Goodman method, the Eq. (8) is fitted to a family of S-N curves with different stress ratios R.

For the purpose of this study, the following equation for a S-N curve proposed in [39] was used as a basis:

$$\frac{\sigma_a}{\sigma_{lim}^f} = 1 + \frac{f_3}{(N_\star + f_2)^{f_1}}, \tag{9}$$

where $N_\star$ is a number of cycles to fatigue failure, σ_a is an alternating stress, and f_1, f_2 and f_3 are fitting parameters. This equation provides a smooth transition of the S-N curve into the horizontal plateau of σ_{lim}^f. Hence, it requires only introduction of the UTS σ_u, which is implemented as

$$\sigma_a(N_\star) = \sigma_{lim}^f + \left(\sigma_u - \sigma_{lim}^f\right)\left[1 - \frac{N_\star^{f_3} - 1}{N_\star^{f_3} + f_2}\right]^{f_1}$$
$$\Leftrightarrow \tag{10}$$
$$N_\star(\sigma_a) = \left(\left[\frac{\sigma_u - \sigma_{lim}^f}{\sigma_a - \sigma_{lim}^f}\right]^{\frac{1}{f_1}}(1 + f_2) - f_2\right)^{\frac{1}{f_3}}.$$

The proposed modification (10) is more convenient than the original formulation (9), and it is a reasonable alternative to previously available equations (7) and (8) because:

– it produces a fully adjustable reverse sigmoidal shape with a mathematical minimum of fitting parameters;
– it contains an upper and lower bounds as σ_{u} and $\sigma^{\mathrm{f}}_{\mathrm{lim}}$;
– it is fully reversible.

Using a previously suggested assumption, a S-N curve lower bound $\sigma^{\mathrm{f}}_{\mathrm{lim}}$ in Eqs (7, 8, 10) can be replaced with $\sigma^{\mathrm{c}}_{\mathrm{y}}$. This would let to identify two material parameters (σ_{u} and $\sigma^{\mathrm{c}}_{\mathrm{y}}$) from tensile and cyclic experiments correspondingly rather than from fatigue tests. The efficiency of Eq. (10) for description of S-N curves is demonstrated in Fig. 3 in application to ASTM A36 steel with σ_{u} from [21] and AISI 4340 steel with σ_{u} from [22]. For both steels $\sigma^{\mathrm{c}}_{\mathrm{y}}$ is taken from Table 2. Identification of the fatigue fitting parameters (f_1, f_2 and f_3) is implemented in Microsoft Excel using an add-in Solver in the same way as described previously for fitting of cyclic and monotonic SSCs by the Chaboche model. All parameters for the S-N curves are reported in Table 3. Finally, the whole range of mathematical formulations for S-N curves is discussed by Castillo & Fernández-Canteli [40].

3.2 Creep behaviour at elevated temperature

Engineering structures operating under constant loading conditions at high temperature are usually designed against the creep failure using the conventional time-to-failure approach. This approach involves experimental creep rupture curves with stress vs. time to failure $t_\star$. A typical creep rupture curve is a trilinear smoothed curve in double logarithmic coordinates, with two inflections corresponding to $\sigma^{\mathrm{c}}_{\mathrm{y}}$ and $\sigma^{\mathrm{m}}_{\mathrm{y}}$. These inflections separate three sections on the creep rupture curve, which are characterised by three different creep damage accumulation modes – brittle, ductile and mixed. Three sections with different creep deformations mechanisms can be typically observed on the minimum creep rate curve, presenting minimum creep strain rate vs. stress, which is also a trilinear smoothed curve in double logarithmic coordinates. The deformations mechanism (linear creep, power-law creep and power-law breakdown) are separated by the same two inflections. This assumption is confirmed by the experiments for ASTM P91 steel at elevated temperatures and corresponding theoretical developments.

Previously, the creep modelling using different creep exponent values in different stress ranges was studied by Gorash *et al.* [15–17]. These studies were devoted to the formulation of constitutive creep model, called double power law and applied to ASTM P91 steel at 600°C:

$$\dot{\varepsilon}^{\mathrm{cr}}(\sigma) = C\frac{\sigma}{\sigma^{\mathrm{cr}}_\star} + C\left(\frac{\sigma}{\sigma^{\mathrm{cr}}_\star}\right)^n = C\frac{\sigma}{\sigma^{\mathrm{cr}}_\star}\left[1+\left(\frac{\sigma}{\sigma^{\mathrm{cr}}_\star}\right)^{n-1}\right], \tag{11}$$

where $\sigma^{\mathrm{cr}}_\star = 100$ MPa is a material parameter called "transition stress", which characterises a transition from linear creep to power creep. Other material parameters were identified as $n = 12$ and $C = 2.5\cdot 10^{-7}$ MPa^{-1}/h.

To implement two transitions into the constitutive model, Eq. (11) is modified by adding the third "power-law breakdown" component to become the triple power law:

$$\dot{\varepsilon}^{\mathrm{cr}}(\sigma) = C_1\sigma^{n_1} + C_2\sigma^{n_2} + C_3\sigma^{n_3} = C\frac{\sigma}{\sigma^{\mathrm{cr}}_\star} + C\left(\frac{\sigma}{\sigma^{\mathrm{cr}}_\star}\right)^n + C\left(\frac{\sigma}{2\,\sigma^{\mathrm{cr}}_\star}\right)^{2n} = C\frac{\sigma}{\sigma^{\mathrm{cr}}_\star}\left[1+\left(\frac{\sigma}{\sigma^{\mathrm{cr}}_\star}\right)^{n-1} + \frac{1}{2}\left(\frac{\sigma}{2\,\sigma^{\mathrm{cr}}_\star}\right)^{2\,n-1}\right], \tag{12}$$

where $\sigma^{\mathrm{cr}}_\star$ is a transition stress, C and n are secondary creep parameters, which have the temperature dependence expressed by Arrhenius-type functions as follows [43]:

$$\sigma^{\mathrm{cr}}_\star(T) = \sigma^{\mathrm{cr}}_{\star 0}\ \exp\left(\frac{Q_\sigma}{R\,T}\right) \quad [\mathrm{MPa}] \tag{13}$$

with $\sigma_\star = 0.0587$ [MPa] and $Q_\sigma = 54100$ [J/mole],

$$C(T) = 10^{-C_0\ \exp\left(\frac{Q_C}{R\,T}\right)} \quad \left[\frac{1}{\mathrm{h}}\right] \tag{14}$$

with $\sigma_C = 1.9916$ [1/h] and $Q_C = 8757.1$ [J/mole],

$$n(T) = n_0\ \exp\left(\frac{Q_n}{R\,T}\right) \tag{15}$$

with $n_0 = 0.2479$ and $Q_n = 28648.4$ [J/mole].

In notations (13)-(15): T is a temperature in K; Q_σ, Q_C and Q_n are creep activation energies and $R = 8.314$ [J · mol^{-1} · K^{-1}] is the universal gas constant. The transition stress $\sigma^{\mathrm{cr}}_\star(T)$ and creep parameters $C(T)$ and $n(T)$ were obtained by fitting the data for minimum creep strain rate from studies by Sklenička *et al.* [42], Kloc & Fiala [41] and Kimura [30] and shown in Fig. 4. The inflections of corresponding curves are observed at 550, 600 and 650°C and explained in terms of transition between different creep deformation mechanisms. Comparison of $\sigma^{\mathrm{cr}}_\star$ defined by Eq. (13) and reported in Table 4 with $\sigma^{\mathrm{c}}_{\mathrm{y}}$ from Table 2 reveals that they are close. As summarised in Table 4, the accuracies are 26.7, 6.4 and 19.2% corresponding to 550, 600 and 600°C.

Another important observation was done in [15–17] for creep rupture behaviour of this steel. The creep-rupture

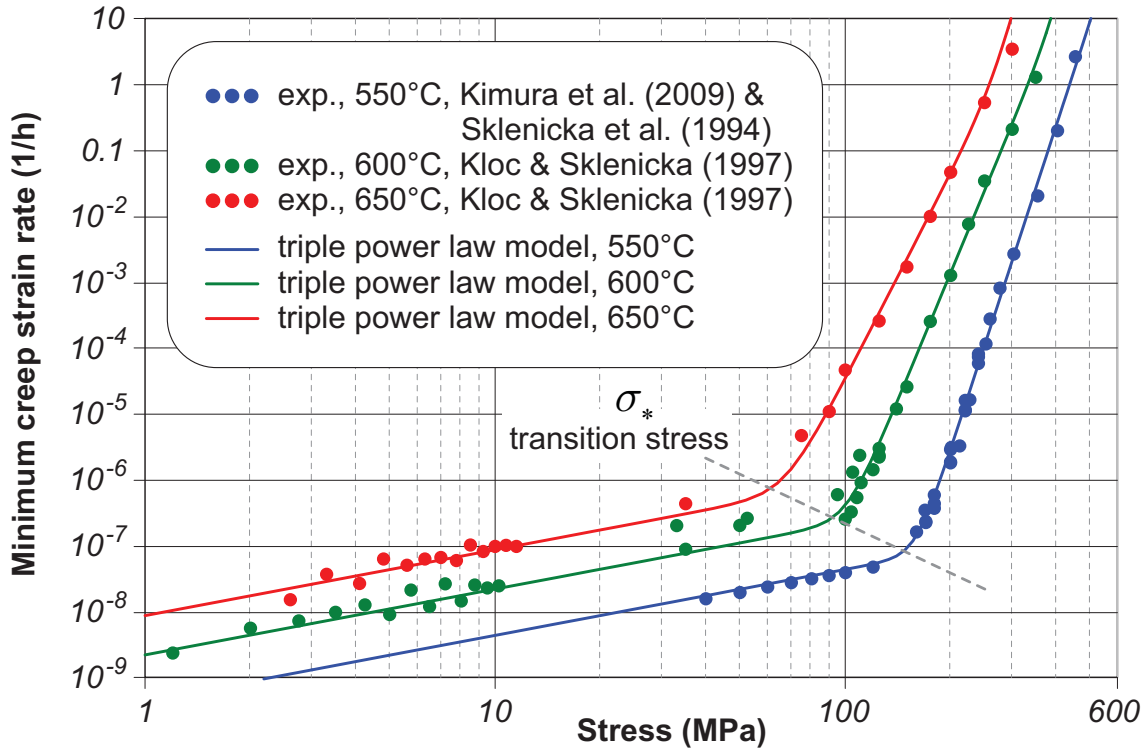

Figure 4: Min. creep rate vs. stress of ASTM P91 steel based on several sets of data [30, 41, 42]

curve, which describes the dependence of time to rupture on stress, exhibits the distinctive inflection too. This inflection is explained as a transition from ductile character of rupture to brittle. This transition was observed at the approximately same stress as the inflection of min. creep rate – $\sigma_{\star}^{\mathrm{cr}} = 100$ MPa at 600°C. Recently, Kimura [14] observed inflections of the experimental curves at 600 and 650°C as shown in Fig. 5 and explained them in terms of half monotonic yield ($\sigma_{\mathrm{y}}^{0.2\%}/2$). In contrast to Kimura's idea [14], in this study, inflections are defined by $\sigma_{\star}^{\mathrm{cr}}$ using Eq. (13). The creep constitutive model (12) is inserting into the Monkman-Grant relationship as in previous work [43] to produce the time to rupture $t_{\star}$:

$$t_{\star}(\sigma, T) = k_1 \left[\dot{\varepsilon}^{\mathrm{cr}}(\sigma, T)\right]^{-k_2}, \tag{16}$$

where $k_1 = 0.23\ \left[1/\mathrm{h}\right]^{k_2-1}$ and $k_2 = 0.83$ are the tertiary creep constants for the ASTM P91 steel, which are identified by fitting equation (16) to the creep-rupture experimental data [14] for the temperature range from 550°C to 650°C.

It should be noted that Dimmler *et al.* [44] associated these inflections with the microstructurally determined threshold stresses (back-stress concept). The applicability of this concept was shown using the experimental minimum creep rate and creep rupture curves for several 9-12%Cr heat resistant steels (P91, GX12, NF616, X20 and B2). Dimmler *et al.* [44] emphasised that the knowledge of these threshold stresses limits the range of experimentally based predictions, thus preventing from overestimation of the long-term creep rate and creep strength from extrapolated short-term creep data.

Since the inflections are captured reasonably well on both types of creep data in Figs 4 and 5, the transition stresses on min. creep rate curves and creep rupture curves proposed by Gorash *et al.* [15–17] can be explained by relating them to $\sigma_{\mathrm{y}}^{\mathrm{c}}$. Therefore, these observations prove that the most safe creep design is guaranteed in linear creep domain with brittle failure mode, which is also defined by the $\sigma_{\mathrm{y}}^{\mathrm{c}}$.

3.3 Fatigue behaviour at elevated temperature

The fatigue performance of ASTM P91 steel is analysed using the HCF experimental data by Matsumori *et al.* [35] at three different temperatures (RT, 400 and 550°C) illustrated in Fig. 6. From these data, it can be concluded that at elevated temperatures the heat-resistant steels don't exhibit $\sigma_{\mathrm{lim}}^{\mathrm{f}}$ on S-N fatigue curves, which is usually observed at normal temperature. The reason for this is the elimination of purely elastic behaviour at high temperature, since

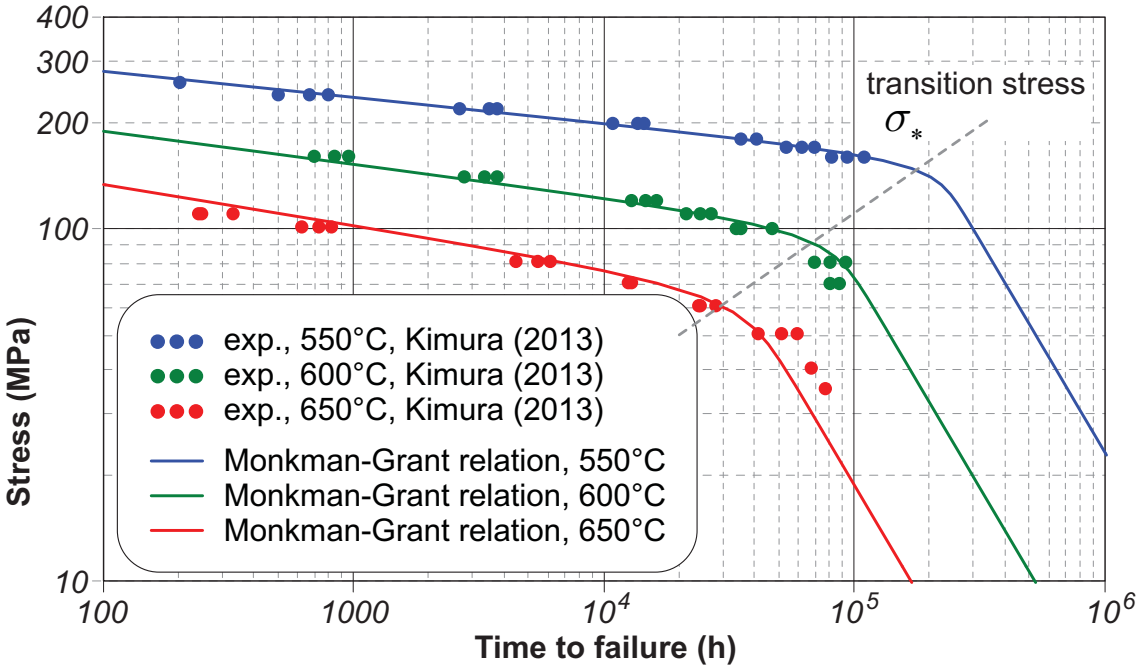

Figure 5: Stress vs. creep rupture life of ASTM P91 steel based on the data by [14]

there is always some amount of inelastic strain, which is caused by creep. Therefore, there is always a permanent accumulation of creep damage, even at low stress levels and high-strain rate, which leads to inevitable failure. This fact is confirmed by the experimental observations [35], which demonstrated the extinction of $\sigma^{\mathrm{f}}_{\mathrm{lim}}$ at 550°C for over 10^8 loading cycles. However, a good match of $\sigma^{\mathrm{f}}_{\mathrm{lim}}$ with $\sigma^{\mathrm{m}}_{\mathrm{y}}$ with accuracy of 2.8% is observed at RT for this steel as shown in Table 4, which makes advanced martensitic steels different from simple ferritic steels for $\sigma^{\mathrm{f}}_{\mathrm{lim}}$ prediction. This effect can be explained by the assumption of Terent'ev [45], who recognised two types of the fatigue endurance limit $\sigma^{\mathrm{f}}_{\mathrm{lim}}$ – standard in HCF range ($N = 10^2$-10^7 cycles) and ultrahigh in giga-cycle fatigue (GCF) range ($N = 10^7$-10^{11} cycles). The existence of ultrahigh $\sigma^{\mathrm{f}}_{\mathrm{lim}}$ was proved by the experimental data for high-strength steels (50CrV4, 54SiCrV6 and 54SiCr6), which demonstrated two inflections of the fatigue curves followed by horizontal plateaus – first in HCF area ($N \approx 10^5$-10^6), second in GCF area ($N \approx 10^8$-10^9). The correspondence of $\sigma^{\mathrm{c}}_{\mathrm{y}}$ with ultrahigh $\sigma^{\mathrm{f}}_{\mathrm{lim}}$ for ASTM P91 steel is expected to be found at $N > 10^8$ cycles, but no experimental data is available for this range.

Following these assumptions, experimental S-N curves for ASTM P91 steel by Matsumori *et al.* [35] are described by the Eq. (10), where $\sigma^{\mathrm{c}}_{\mathrm{y}}$ is replaced by $\sigma^{\mathrm{m}}_{\mathrm{y}}$ as shown in Fig. 6. The experimental values of σ_{u} for all temperatures are taken from [35]. The value of $\sigma^{\mathrm{m}}_{\mathrm{y}}$ for RT is taken from Table 2, while $\sigma^{\mathrm{f}}_{\mathrm{lim}}$ from [35] is taken instead of $\sigma^{\mathrm{m}}_{\mathrm{y}}$ for 400°C, and $\sigma^{\mathrm{f}}_{\mathrm{lim}} = 0$ is assumed for 550°C because of creep. All parameters for the S-N curves are reported in Table 3.

Finally, the values of $\sigma^{\mathrm{m}}_{\mathrm{y}}$ and $\sigma^{\mathrm{c}}_{\mathrm{y}}$ for ASTM P91 steel defined by Chaboche model as shown in Figs 2c and 2d are listed in Table 4. They are plotted versus temperature in Kelvins (K) in Fig. 7. The temperature dependence of a yield strength defined as $\sigma^{\mathrm{el}}_{\mathrm{y}}$ is extrapolated by a simple elliptic equation, which can be assumed as an extension of the von Mises yield criterion by temperature consideration, in the following form:

$$\left(\frac{T}{T_{\mathrm{eut}}}\right)^2 + \left(\frac{\sigma_{\mathrm{y}}}{\sigma_{\mathrm{y0}}}\right)^2 = 1 \quad \Rightarrow \quad \sigma_{\mathrm{y}}(T) = \sigma_{\mathrm{y0}}\sqrt{1 - \left(\frac{T}{T_{\mathrm{eut}}}\right)^2}, \tag{17}$$

where $T_{\mathrm{eut}} = 1000$ K is a typical eutectic temperature for steel alloys; $\sigma^{\mathrm{c}}_{\mathrm{y0}} = 210$ [MPa] and $\sigma^{\mathrm{m}}_{\mathrm{y0}} = 2 \cdot \sigma^{\mathrm{c}}_{\mathrm{y0}} = 420$ [MPa] are theoretical yield strengthes at absolute zero temperature for monotonic and cyclic responses correspondingly. Since it is not possible to measure the values of $\sigma^{\mathrm{m}}_{\mathrm{y0}}$ and $\sigma^{\mathrm{c}}_{\mathrm{y0}}$ experimentally, they can be estimated using the results of only one experimental measurement (for instance, at RT) in Eq. (17). However, the value of $T_{\mathrm{eut}} = 1000$ K is proved experimentally to be an eutectic temperature in the iron-carbon system, which characterises the co-

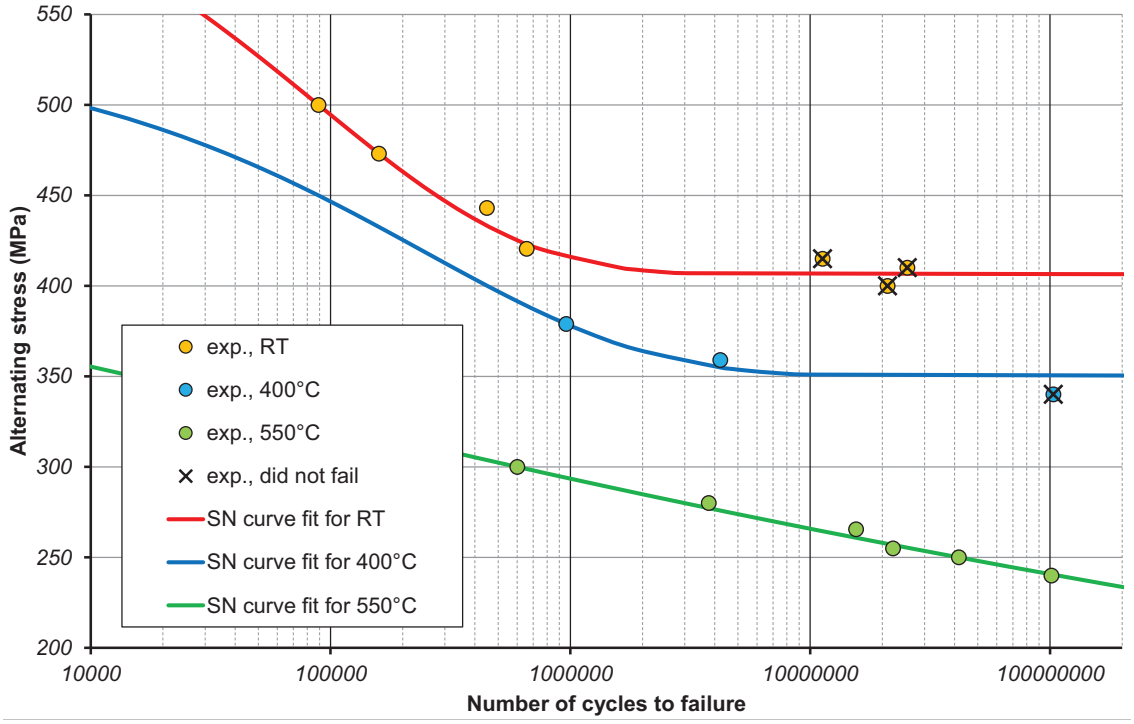

Figure 6: S-N curve fits of ASTM P91 steel based on HCF data by Matsumori *et al.* [35]

existence of solid and liquid phases on iron-carbon phase diagram.

4 Conclusions

This study explains the existence of the fatigue limit $\sigma^{\mathrm{f}}_{\mathrm{lim}}$ and creep transition stress $\sigma^{\mathrm{cr}}_{\star}$ by the cyclic yield strength $\sigma^{\mathrm{c}}_{\mathrm{y}}$ using the fatigue and creep experimental data for a few structural steels at normal and elevated temperatures. The comparison of yield strengths ($\sigma^{\mathrm{m}}_{\mathrm{y}}$, $\sigma^{\mathrm{c}}_{\mathrm{y}}$), $\sigma^{\mathrm{f}}_{\mathrm{lim}}$ and $\sigma^{\mathrm{cr}}_{\star}$ for ASTM A36, AISI 4340 and ASTM P91 steels is summarised in Table 4. Monotonic and cyclic yield strengths ($\sigma^{\mathrm{m}}_{\mathrm{y}}$, $\sigma^{\mathrm{c}}_{\mathrm{y}}$) are defined as elastic limit specified in the scope of the Chaboche model [19, 20]. Fatigue limit $\sigma^{\mathrm{f}}_{\mathrm{lim}}$ of ASTM A36 and AISI 4340 steels complies with $\sigma^{\mathrm{c}}_{\mathrm{y}}$. Equality of $\sigma^{\mathrm{m}}_{\mathrm{y}}$ and $\sigma^{\mathrm{f}}_{\mathrm{lim}}$ at RT for ASTM P91 steel can be explained by the GCF concept [45] introducing two fatigue limits.

Creep transition stress $\sigma^{\mathrm{cr}}_{\star}$ of ASTM P91 steel complies with $\sigma^{\mathrm{c}}_{\mathrm{y}}$. Moreover, Kimura's assumption [14] of half monotonic yield ($\sigma^{0.2\%}_{\mathrm{y}}/2$) agrees very well with the outcomes of the current study. According to Table 4, the relation $\sigma^{\mathrm{c}}_{\mathrm{y}} \approx \sigma^{\mathrm{m}}_{\mathrm{y}}/2$ is valid for all temperatures except the highest 650°C regarding ASTM P91 steel. This assumption is not relevant to AISI 4340 steel, which exhibits $\sigma^{\mathrm{c}}_{\mathrm{y}} \approx \sigma^{\mathrm{m}}_{\mathrm{y}}$.

An important finding is that the temperature dependence of yield strengths ($\sigma^{\mathrm{m}}_{\mathrm{y}}$, $\sigma^{\mathrm{c}}_{\mathrm{y}}$) resembles the von Mises yield criterion, which is elliptic in terms of the principle stresses. In the proposed formulation in form of Eq. (17), the yield surface is also presented by ellipse in coordinates of yield strength and temperature as shown in Fig. 7.

The principal advantage of the $\sigma^{\mathrm{c}}_{\mathrm{y}}$ application to the characterisation of fatigue and creep strength is the relatively fast experimental identification. The total duration of all cyclic tests, which are required to reach the stabilised stress response for the construction of cyclic SSC is much less than the typical durations of fatigue and creep rupture tests at stress levels around $\sigma^{\mathrm{c}}_{\mathrm{y}}$.

The critical point in the work presented here is an application of the advanced material model [19, 20] to the estimation of a single value of elastic limit $\sigma^{\mathrm{el}}_{\mathrm{y}}$, which may seem to be complicated. However, this approach is effective in typical cases when experimental SSCs are unavailable in explicit form, but available in the form of R-O [24] fittings using Eq. (1). In other cases, when all necessary experimental SSCs are available in form of raw data, the modified form (6) of the R-O model proposed by Lemaitre & Chaboche [29] may reduce the fitting procedure just to one step. Since Eq. (6) contains σ_{y} as a material parameter, the application of Chaboche model equations (3)-(5) may no longer be needed.

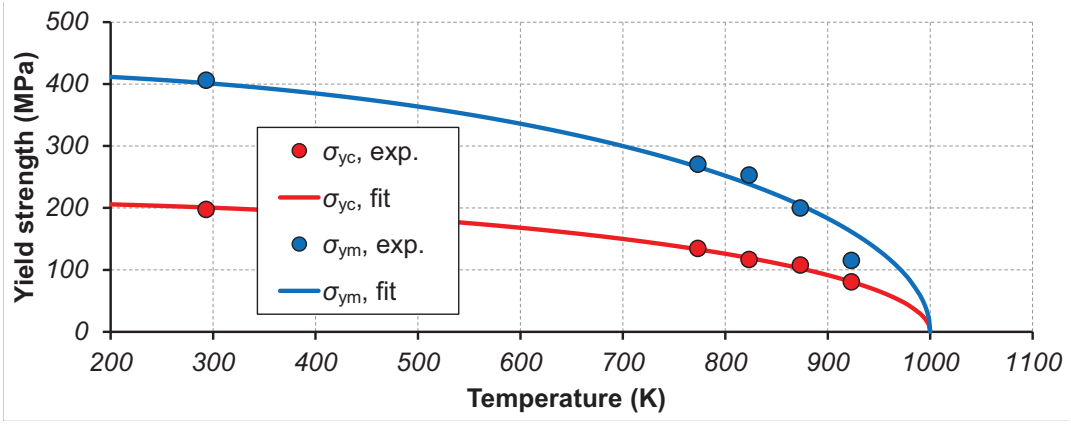

Figure 7: Elliptic yield surfaces of ASTM P91 steel using temperature-dependent σ_y^m and σ_y^c from Table 4.

Table 4: Comparison of σ_y^m, σ_y^c, σ_{lim}^f and $\sigma_\star^{cr}$ for ASTM A36, AISI 4340 and ASTM P91 steels.

Steel	ASTM A36	AISI 4340	ASTM P91					
Temp., °C	RT	RT	RT	400	500	550	600	650
σ_y^m, MPa	248.2	341.2	406.1	–	270.7	253.0	200.0	115.3
σ_y^c, MPa	115.8	330.7	197.5	–	134.5	116.6	107.7	80.6
σ_y^m/σ_y^c	2.1	1.0	2.1	–	2.0	2.2	1.9	1.4
σ_{lim}^f, MPa	160.0	350.0	418.0	350.0	–	–	–	–
$\sigma_\star^{cr}$, MPa	–	–	–	–	–	159.2	101.2	67.6
$\Delta\sigma$, %	27.6	5.5	2.8	–	–	26.7	6.4	19.2

References

[1] Bäumel A., Seeger T., Materials data for cyclic loading: Supplement 1, no. 61 in Materials Science Monographs, Elsevier Science Publishers, Amsterdam, Netherlands, 1990

[2] Manson S.S., Fatigue: A complex subject – Some simple approximations, Exp. Mech., 1965, 5(4), 193–226

[3] Muralidharan U., Manson S.S., A Modified Universal Slopes equation for estimation of fatigue characteristics of metals, J. Eng. Mater. Tech. - T. ASME, 1988, 110(1), 55–58

[4] Boller C., Seeger T., Materials Data for Cyclic Loading: Volumes 1-5, no. 42a-42e in Materials Science Monographs, Elsevier Science Publishers, Amsterdam, Netherlands, 1987

[5] Korkmaz S., Uniform Material Law: Extension to high-strength steels. A methodology to predict fatigue life of high-strength steels, VDM Verlag, Saarbrücken, Germany, 2010

[6] Kim K.S., Chen X., Han C., Lee H.W., Estimation methods for fatigue properties of steels under axial and torsional loading, Int. J. Fatigue, 2002, 24(7), 783–793

[7] Roessle M.L., Fatemi A., Strain-controlled fatigue properties of steels and some simple approximations, Int. J. Fatigue, 2000, 22(6), 495–511

[8] Casagrande A., Cammarota G.P., Micele L., Relationship between fatigue limit and vickers hardness in steels, Mater. Sci. Eng. A, 2011, 528(9), 3468–3473

[9] Bandara C.S., Siriwardane S.C., Dissanayake U.I., Dissanayake R., Fatigue strength prediction formulae for steels and alloys in the gigacycle regime, Int. J. Mat. Mech. Man., 2013, 1(3), 256–260

[10] Li J., Sun Q., Zhang Z.-P., Li C.-W., Qiao Y.-J., Theoretical estimation to the cyclic yield strength and fatigue limit for alloy steels, Mech. Res. Commun., 2009, 36(3), 316–321

[11] Tomasella A., el Dsokia C., Hanselka H., Kaufmann H., A computational estimation of cyclic material properties using Artificial Neural Networks, Procedia Engineer., 2011, 10, 439–445

[12] Pang J.C., Li S.X., Wang Z.G., Zhang Z.F., Relations between fatigue strength and other mechanical properties of metallic materials, Fatigue Fract. Eng. Mater. Struct., 2014, 37(9), 958–976

[13] Bathias C., Fatigue limit in metals, Wiley-ISTE, London, UK, 2014

[14] Kimura K., Creep rupture strength evaluation with region splitting by half yield, in: Proc. ASME 2013 PVP Conf., no. 97819 in PVP2013, ASME, Paris, France, 2013, 1–8

[15] Gorash Y., Development of a creep-damage model for non-isothermal long-term strength analysis of high-temperature components operating in a wide stress range, PhD thesis, Center of Engineering Sciences, Martin-Luther-University Halle-Wittenberg, Halle (Saale), Germany, 2008

[16] Altenbach H., Gorash Y., Naumenko K., Steady-state creep of a pressurized thick cylinder in both the linear and the power law ranges, Acta Mechanica, 2008, 195(1-4), 263–274

[17] Gorash Y., Development of a creep-damage model for a wide stress range, SVH-Verlag, Saarbrücken, Germany, 2015

[18] Dowling N.E., Mechanical Behavior of Materials: Engineering Methods for Deformation, Fracture, and Fatigue, 4th ed., Pearson Education Limited, Harlow, UK, 2013

[19] Chaboche J.-L., Dang Van K., Cordier G., Modelization of the strain memory effect on the cyclic hardening of 316 stainless

steel, in: Trans. 5th Int. Conf. on Structural Mechanics in Reactor Technology, no. L11/3 in SMiRT5, 1–10, IASMiRT, Berlin, Germany, 1979
[20] Chaboche J.-L., A review of some plasticity and viscoplasticity constitutive theories, Int. J. Plasticity, 2008, 24(10), 1642–1693
[21] Higashida Y., Lawrence F.V., Strain controlled fatigue behavior of weld metal and heat-affected base metal in A36 and A514 steel welds, FCP Report No. 22, University of Illinois, Urbana, Illinois, USA, 1976
[22] Smith R.W., Hirschberg M.H., Manson S.S., Fatigue behavior of materials under strain cycling in low and intermediate life range, Technical Note No. D-1574, NASA, Cleveland, Ohio, USA, 1963
[23] NRIM Fatigue Data Sheet No. 78, Data sheets on elevated-temperature, time-dependent low-cycle fatigue properties of ASTM A387 Grade 91 (9Cr-1Mo) steel plate for pressure vessels, Tech. rep., National Research Institute for Metals, Tokyo, Japan, 1993
[24] Ramberg W., Osgood W.R., Description of stress-strain curves by three parameters, Technical Note No. 902, NASA, Washington DC, USA, 1943
[25] Armstrong P.J., Frederick C.O., A mathematical representation of the multiaxial Bauschinger effect, Report no. RD/B/N731, CEGB, Berkeley, UK, 1966
[26] Microsoft® Office Professional Plus, Excel Help System // Analyzing data // What-if analysis // Define and solve a problem by using Solver, Microsoft Corp., Release 2010 ed., 2009
[27] Hyde T., Sun W., Hyde C., Applied Creep Mechanics, McGraw-Hill Education, New York, USA, 2004
[28] ASTM Standard, Standard Specification for Carbon Structural Steel, no. A36/A36M – 08 in ASTM, ASTM International, West Conshohocken, USA, 2008
[29] Lemaitre J., Chaboche J.-L., Mechanics of Solid Materials, Cambridge University Press, Cambridge, UK, 1994
[30] Kimura K., Kushima H., Sawada K., Long-term creep deformation property of modified 9Cr-1Mo steel, Mater. Sci. Eng. A, 2009, 510-511, 58–63
[31] Wang X.G., Crupi V., Guo X.L., Zhao Y.G., Quantitative thermographic methodology for fatigue assessment and stress measurement, Int. J. of Fatigue, 2010, 32(12), 1970–1976
[32] Boyer H.E., Atlas of Fatigue Curves, ASM International, Materials Park, Ohio, USA, 1986
[33] Dowling N.E., Mean stress effects in Stress-Life and Strain-Life fatigue, SAE Technical Paper, 2004, 2004-01-2227, 1–14
[34] Ragab A., Alawi H., Sorein K., Corrosion fatigue of steel in various aqueous environments, Fatigue Fract. Eng. Mater. Struct., 1989, 12(6), 469–479
[35] Matsumori Y., Nemoto J., Ichikawa Y., Nonaka I., Miura H., High cycle fatigue properties of modified 9Cr-1Mo steel at elevated temperatures, in: Proc. ASME 2012 Int. Mechanical Engineering Congress & Exposition, no. 87329 in IMECE2012, ASME, Houston, Texas, USA, 2012, 85–89
[36] Basquin O., The exponential law of endurance tests, Proc. ASTM, 1910, 10(II), 625–630
[37] Bastenaire F., New method for the statistical evaluation of constant stress amplitude fatigue-test results, in: R.A. Heller (Ed.), Probabilistic Aspects of Fatigue, no. STP 511 in ASTM special technical publication, chapter 1, 3–28, ASTM, Philadelphia, USA, 1972
[38] Newbold P., ANSYS® nCode DesignLife Theory Guide, HBM nCode, Catcliffe, Rotherham, UK, Release 15.0 ed., 2013
[39] Newbold P., ANSYS® nCode DesignLife Worked Examples, HBM nCode, Catcliffe, Rotherham, UK, Release 15.0 ed., 2013
[40] Castillo E., Fernández-Canteli A., A unified statistical methodology for modeling fatigue damage, Springer, Berlin, Germany, 2009
[41] Kloc L., Sklenička V., Transition from power-law to viscous creep behaviour of P-91 type heat-resistant steel, Mater. Sci. Eng. A, 1997, A234-A236, 962 – 965
[42] Sklenička V., Kuchařová K., Dlouhý A., Krejčí J., Creep behaviour and microstructure of a 9cr steel, in: D. Coutsouradis et al. (Ed.), Proc. Conf. Materials for Advanced Power Engineering 1994: Part I, Kluwer Academic Publishers, Liège, Belgium, 1994, 435–444
[43] Gorash Y., Altenbach H., Lvov G., Modelling of high-temperature inelastic behaviour of the austenitic steel aisi type 316 using a continuum damage mechanics approach, J. of Strain Analysis for Eng. Design, 2012, 47(4), 229–243
[44] Dimmler G., Weinert P., Cerjak H., Extrapolation of short-term creep rupture data – The potential risk of over-estimation, Int. J. Pres. Ves. Pip., 2008, 85, 55–62
[45] Terent'ev V.F., Endurance limit of metals and alloys, Met. Sci. Heat Treat., 2008, 50(1-2), 88–96

Nomenclature

Abbreviations

GCF	Giga-Cycle Fatigue
HCF	High-Cycle Fatigue
MUS	Method of Universal Slopes
R-O	Ramberg-Osgood
RT	room temperature
SSC	Stress-Strain Curve
UML	Uniform Material Law
UTS	Ultimate Tensile Strength

Variables, Constants

σ	stress
$\Delta\sigma$	stress range
σ_{a}	alternating stress
$\bar{\sigma}$	mean stress of the cycle
$\sigma_{\max}$	maximum stress in the cycle
σ_{y}	yield strength
σ_{y0}	yield strength at absolute zero
$\sigma_{\mathrm{y}}^{\mathrm{c}}$	cyclic yield strength
$\sigma_{\mathrm{y}}^{\mathrm{m}}$	monotonic yield strength
$\sigma_{\mathrm{y}}^{\mathrm{p}}$	proportional limit
$\sigma_{\mathrm{y}}^{\mathrm{el}}$	elastic limit
$\sigma_{\mathrm{y}}^{0.2\%}$	offset yield strength

$\sigma^{\mathrm{f}}_{\mathrm{lim}}$	fatigue endurance limit
σ_{u}	ultimate tensile strength
$\sigma^{\mathrm{cr}}_{\star}$	creep transition stress
ε	strain
$\dot{\varepsilon}$	strain rate
$\Delta\varepsilon$	strain range
ε_{f}	true fracture ductility
$\varepsilon^{\mathrm{tot}}$	total strain
ε^{p}	plastic strain
ψ	reduction in area
HV	Vickers hardness
HB	Brinnell hardness
R^2	coefficient of determination
E	Young's (elasticity) modulus
B, β	R-O model constants
X_i	kinematic backstresses
C_i, γ_i	kinematic material constants
$N_\star$	number of cycles to fatigue failure
$t_\star$	time to creep failure
A, B, C	fatigue parameters for Bastenaire model
a, b, c, α	fatigue parameters for Chaboche model
f_1, f_2, f_3	fatigue parameters for Chaboche model
C, n	secondary creep parameters
Q_σ, Q_C, Q_n	creep activation energies
k_1, k_2	secondary creep parameters
T	temperature
T_{eut}	eutectic temperature

Subscripts, Superscripts

y	yield
c	cyclic
a	alternating
m	monotonic
cr	creep
f	fatigue
el	elastic
p	plastic
$\star$	failure
tot	total
lim	limit
u	UTS
eut	eutectic